

2 Thin film growth

2.1 Nucleation and epitaxy

Epitaxy is the deposition of a single crystalline film on a single crystal substrate²⁷. Thin films are layers of material on a substrate with thicknesses ranging from a fraction of a nanometre to some micrometers²⁸. Thin film properties often differ from bulk properties due to different defect structures, their quasi two-dimensionality (ultrathin films) and the strong influence of surface and interface effects. Thin film growth is influenced by a large variety of physical effects like thermodynamics and kinetics, crystallography, as well as electronic, mechanic and magnetic properties. The grain size of the thin film or the domain size of the first layer is mostly determined by the deposition rate and the substrate temperature, which affect the nucleation and diffusion of the adsorbates²⁹. High temperature and/or low deposition rate result in large crystal grains/domains, while low temperature and/or high deposition rate lead to small grains/domains.

In UHV conditions, three steps in the deposition of material on a surface can be distinguished: (i) emission of the material (e.g. atoms, molecules or ion pairs) by sublimation, (ii) collision free transfer of the material to the surface, (iii) condensation on the surface. The third step mostly determines the thin film growth and can be viewed as a multi step process²⁹: (i) energy loss of the impinging particles to stay on the surface, (ii) binding to the surface (either physisorption or chemisorption), (iii) surface diffusion and cluster formation, (iv) nucleation, (v) island growth, (vi) coalescence of the islands, (vii) continued three-dimensional growth of the islands. During the nucleation small numbers of particles meet and arrange in a crystalline pattern. Thereby, they form sites where additional particles can be trapped and initiate the growth process³⁰. The initial nucleation usually takes place at defects like steps, kinks or dislocations due to the lower coordination sites, which exhibit a higher desorption barrier of the particles at these defects.

2.2 Growth modes of thin films

In general, there exist three different growth modes of epitaxial films as illustrated in Figure 1. These growth modes depend on the lattice misfit, on the differences in the binding energies between the particles and between particles and the surface, on diffusion and on the surface tension. For the Volmer-Weber (island) growth mode (cf. Figure 1, right) the interaction between the particles is stronger than the interaction between particles and surfaces. In contrast, in the Frank van der Merwe growth mode the adsorbates bind more strongly to the surface which results in a layer by layer growth (cf. Figure 1, left). The

2 THIN FILM GROWTH

Stransky-Krastanov growth mode is an intermediary process, where a layer-by-layer growth, i.e. the formation of a wetting layer with thicknesses up to several monolayers, is followed by island growth on top of the wetting layer (cf. Figure 1, centre). Stransky-Krastanov growth usually results from the strain, induced in the first monolayers, due to the lattice misfit.



Figure 1: Different thin film growth modes as described in the text.

3 Experimental techniques and set-up

3.1 Experimental techniques

In this thesis several complementary surface sensitive techniques, like STM and STS, XPS, UPS and LEED have been used. This chapter provides an introduction into these techniques and into some particularities, which are necessary for the interpretation of the data.

3.1.1 Scanning tunnelling microscopy and spectroscopy

The scanning tunnelling microscope (STM) was invented in 1982 by Binnig and Rohrer¹⁵, who were honoured with the Noble prize in 1986. The invention of a microscope, which provides a three-dimensional real space image of a surface with atomic resolution, allowed spatially localized investigation of the electronic and geometric properties of surfaces. The invention of the STM gave rise to several further scanning probe techniques like atomic force microscopy, magnetic force microscopy and chemical force microscopy, which expanded the field of surface science. With the wide parameter-sets possible for all scanning probe techniques, like variable temperature and variable pressure, different physical and chemical information can be acquired. SPMs are used (i) to access electronic states of surface adsorbates with a very good lateral resolution³¹, (ii) to directly investigate chemical reactions at the solid liquid interface³² and (iii) to laterally and chemically manipulate³³ adsorbates on surfaces. For a detailed description of the various scanning probe techniques the reader is referred to several text books^{34,35}.

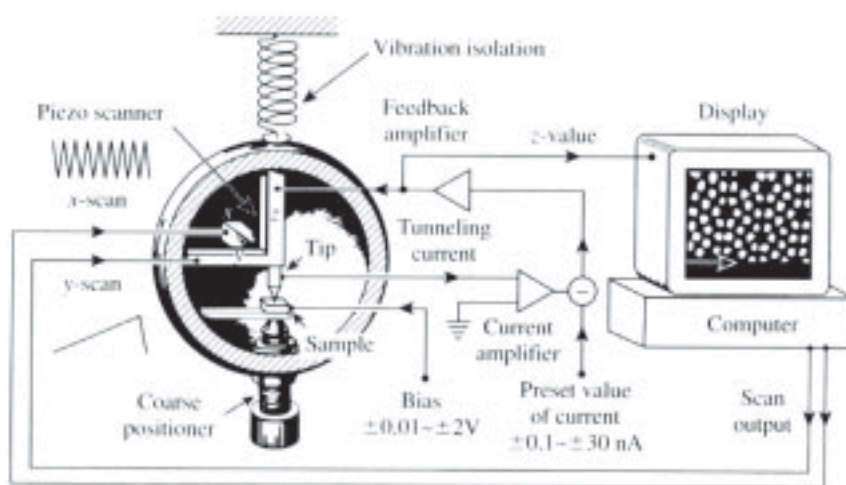


Figure 2: Set-up of an STM from³⁴.

3 EXPERIMENTAL TECHNIQUES AND SET-UP

The set-up of a scanning tunnelling microscope is shown in Figure 2. An STM tip usually made of electrochemically etched W or wire-cut PtIr is attached to a three-piezo scanner (x, y and z) or a piezo tube. A bias voltage is applied between the tip and the sample to establish a tunnelling current, when the tip is in close proximity to the surface (~ 1 nm). By using piezoelectric actuators the tip scans the surface line by line with a very high local accuracy. The tunnelling current measured at each point is amplified and compared to a reference value. Using the z-piezo actuator to adjust the tip elevation above the substrate the tunnelling current can be kept constant. Thus, a topographic image of the surface can be acquired by plotting the z-position in dependence of the x- and y- position of the tip, as seen in the display in Figure 2. This measurement technique is called constant current mode. Another measurement method is the so called constant height mode. Here the z-position of the tip is kept constant and the current in dependence on the x- and y-position is displayed directly. For the latter technique higher scanning speeds can be achieved because the z-displacement does not need to be adjusted via the feedback loop. Therefore, a higher resolution can be obtained, but it is limited to very flat surfaces otherwise the tunnelling contact may be lost or the tip may crash into the surface. For atomic resolution a sufficient damping and vibration isolation between the microscope and the environment is necessary.

In the following, a brief overview of the electronic nature of the tunnelling process will be given. Figure 3 shows schematically the energy diagram of a vacuum tunnelling barrier between an STM tip (T) and the sample (S). The density of states (DOS) of the tip is assumed to be featureless near the Fermi energy whereas the density of states of the sample varies with energy, which is usually the case for semiconducting samples or organic adsorbates. In Figure 3a the absolute value of two wave functions with different energies are displayed and both decay exponentially in the vacuum with the decay length of the lower lying states being smaller (cf. equation 1). When the tip and the sample are separated the vacuum levels of both are equal; the position of the Fermi level (E_{Fermi}) is given by the work function (Φ) of the tip and the sample, respectively. When both are brought to close contact (usually 0.5-5 nm distance between the tip and the sample for STM measurements), tunnelling of electrons between both materials is possible and the Fermi levels in the thermal equilibrium are aligned, resulting in a change of the vacuum level of the sample with respect to the vacuum level of the tip (Figure 3b). When a negative voltage V is applied to the tip a rigid shift of the energy states of the tip with respect to the energy states of the sample by approximately eV occurs. This results in a net tunnelling current from the occupied states of the tip into the unoccupied states of the sample (Figure 3c). When a positive voltage is applied to the tip a tunnelling current in the opposite direction, i.e. out of occupied states of the sample into unoccupied states of the tip occurs (Figure 3d). The arrows in Figure 3c and d indicate the tunnelling probability depending on the energy of the electrons according to equation 1. Thus, the main contribution to the tunnelling current results from the highest lying states due to the energy dependent decay length of the electron wave functions as indicated in Figure 3a.

$$\Psi \approx \exp(-\kappa d) \quad \kappa = 2\sqrt{-2mE}/\hbar \quad (1)$$

3.1 Experimental techniques

By changing the applied bias it is possible to spectroscopically measure the occupied and unoccupied states of the sample. Figure 3d shows that it is difficult to detect the lower lying occupied states (HOMO-1, HOMO-2) of the sample because the biggest amount of the tunnelling current results from the states near the Fermi energy and the contribution of lower lying states to the tunnelling current is comparably small. In consequence, the unoccupied states can be easier detected with scanning tunnelling spectroscopy (STS) than the occupied states. To directly acquire the DOS of the sample scanning tunnelling spectroscopy can be performed by placing the tip on top of the point of interest, switching off the feedback loop and measuring a current/voltage curve. Due to the dependence of the tunnelling spectra on the DOS of the tip it is often advantageous, if not essential, to compare the scanning tunnelling spectra with complementary analysis methods like UPS, NEXAFS and/or IPES.

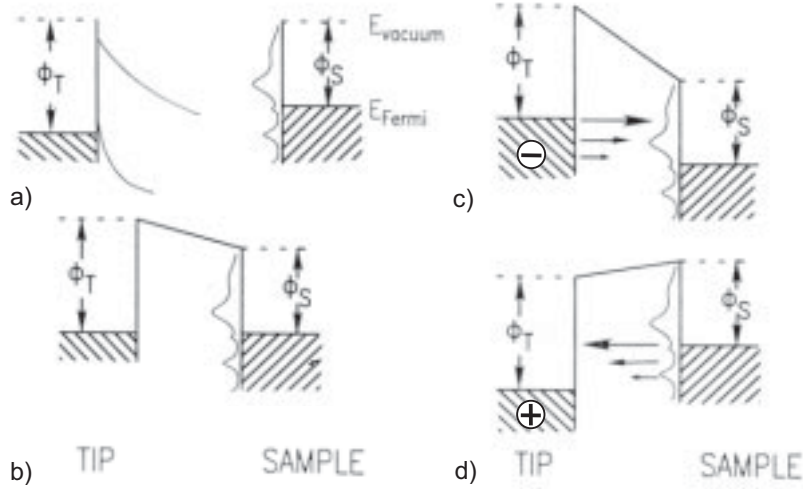


Figure 3: Energy diagram of the vacuum tunnelling barrier between the STM tip and the sample a) tip and sample separated, b) tip and sample in close contact, c) negative voltage applied to the tip, d) positive voltage applied to the tip; from³⁵.

To estimate the tunnelling current the Wentzel–Kramers–Brillouin (WKB) approximation can be applied as shown in equation 2: d is the distance between the tip and the sample, m is the electron mass and V is the applied tunnelling voltage.

$$i(d, V) \cong \frac{2\pi e}{\hbar} \left(\frac{\hbar^2}{2m} \right)^2 \int_0^{eV} \rho_s(E) \rho_t(E - eV) T(d, V, E) dE \quad (2)^{36}$$

Thus, the tunnelling current density depends on the DOS of the sample (ρ_s), on the DOS of the tip (ρ_t) and on the transmission function T , which is given in equation 3.

$$T(d, eV, E) = \exp \left(- \frac{2d\sqrt{2m}}{\hbar} \sqrt{\frac{\Phi_s + \Phi_t}{2} + \frac{eV}{2} - E} \right) \quad (3)^{36}$$

3 EXPERIMENTAL TECHNIQUES AND SET-UP

Equation 2 shows that the tunnelling current directly depends on the DOS of the sample, as already discussed in the previous paragraph. Thus, to study the DOS of a sample one can differentiate the tunnelling current. Assuming a constant DOS of the tip and a slowly changing transmission function the derivative of the tunnelling current can be approximated according to equation 4. The tip quality and the density of states of the tip is usually controlled by measuring tunnelling spectra on the clean well-known substrate.

$$\frac{\partial i(d,V)}{\partial V} \approx \rho_t(0)\rho_s(E)T(d,V,eV) \quad (4)^{36}$$

3.1.2 Photoelectron spectroscopy

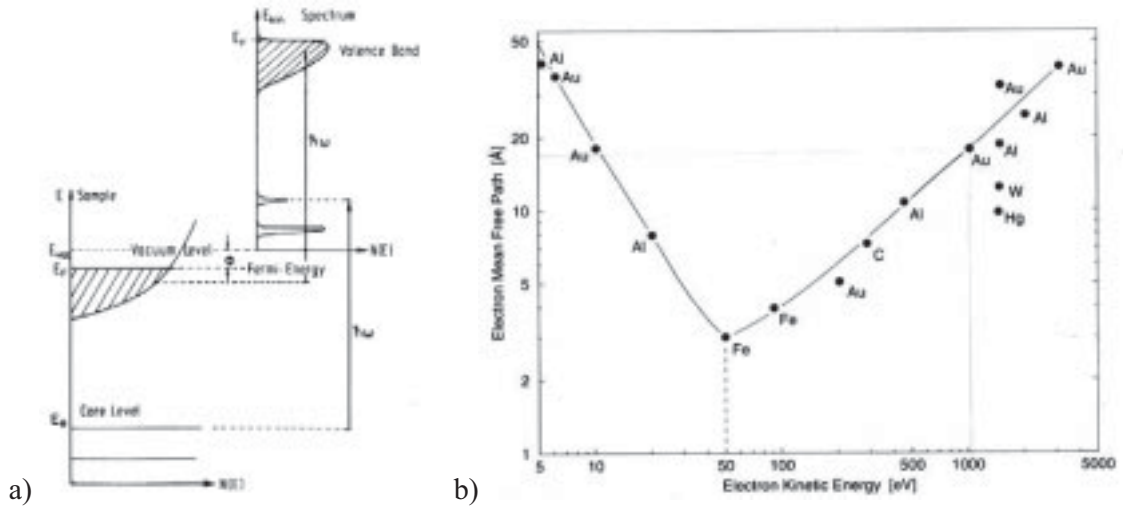


Figure 4: a) relation between the energy levels of a solid and the resulting electron energy distribution; b) electron mean free path depending on the electron kinetic energy; from³⁷.

The phenomenon of photoemission of electrons from materials was already discovered in 1887 by Hertz³⁸ and in 1905 Einstein delivered the explanation of this so called photoelectric effect using the quantum nature of light³⁹. The photoemission process and the resulting photoemission spectrum is schematically depicted in Figure 4a. A sample is irradiated with photons with a well defined energy $\hbar\omega$. The energy is transferred to the electrons of the material and as a consequence the electrons can leave the material with a kinetic energy (E_{kin}) which is given in equation 5, where E_{bind} is the binding energy of the electron with respect to the Fermi energy and Φ is the work function of the sample. Due to the relatively small electron mean free path for electron kinetic energies between 50 and 1000 eV (cf. Figure 4b) this technique is highly surface sensitive and thus very well suited for studying adsorbates on surfaces. Due to the element specific binding energy of the electrons this technique is also called Electron Spectroscopy for Chemical Analysis (ESCA). One main application area for

3.1 Experimental techniques

ESCA is the determination and quantification of the elemental composition of unknown materials.

$$E_{\text{kin}} = h\nu - E_{\text{bind}} - \Phi \quad (5)$$

The photoemission process can be described by a three step model. In the first step the photo-ionization takes place, i.e. the electron is excited. In a second step this electron is transported to the surface and finally the electron escapes from the surface into the vacuum in the third step. During the transport of the electron to the surface inelastic scattering of the electron can take place resulting in a decrease of the kinetic energy. This results in an increasing background with increasing binding energy of the photoemission spectra. The three step model is a rather simple picture and the photo-ionization, i.e. the first step of this model is actually more complex because it has to be viewed as a many-body process. After removal of the electron from the N -electron system a positively charged hole remains which leads to a $(N-1)$ -final state. Usually the binding energy of the emitted electron calculated by equation 5 is smaller than the real binding energy due to the different energy of the $(N-1)$ -system compared to the N -system. During the relaxation of the excited system the relaxation energy is released and can be transferred to the photoelectron to increase its kinetic energy. In consequence one has to rewrite equation 5 like it is done in equation 6:

$$E_{\text{kin}} = h\nu - (E_f^{N-1} - E_i^N) - \Phi \quad (6)$$

The measured effective binding energy ($E_{\text{b,eff}}$) depends on several terms as shown in equation 7⁴⁰:

$$E_{\text{b,eff}} = E_{\text{b}}(\text{atom}) + \Delta E_{\text{chem}} + \Delta E_{\text{Mad}} + \Delta E_{\text{r,int}} + \Delta E_{\text{r,ext}} \quad (7)$$

The chemical shift ΔE_{chem} describes the effective charge of the atom and the influence of the nearest neighbours to the binding energy of the electron. If the atom is surrounded by electronegative neighbours, the electrons are attracted by the neighbouring atoms which results in a higher binding energy of the core electrons. This effect can be well seen for halide-containing molecules. For example, the binding energy of the C1s electron of CF_4 is 296.7 eV compared to CHF_3 which has a binding energy of 294.7 eV⁴¹. The chemical shift is a very important factor for determining the chemical composition of unknown materials, especially for polymers and organic molecules.

The Madelung term ΔE_{Mad} is only valid for ionic crystals and describes the electric potential of all lattice components at the central atom. For ionic crystals the Madelung term can often completely compensate the chemical shift.

The relaxation energies consider the multi-particle effects which lead to a larger kinetic energy of the photoelectrons. Generally, the relaxation can be divided into two factors the internal relaxation $\Delta E_{\text{r,int}}$ and the external relaxation $\Delta E_{\text{r,ext}}$. The latter term considers the polarizability of the medium surrounding the atom. The local positive charge of the photohole can be screened by attraction of the surrounding electrons. The internal relaxation ($\Delta E_{\text{r,int}}$) results from a shifting of the electronic orbitals towards the core as well from relaxation of the

3 EXPERIMENTAL TECHNIQUES AND SET-UP

excited system by filling of the photohole with an electron from a higher orbital. Parts of this relaxation energy can be transferred to the photoelectron which results in a higher kinetic energy and in consequence in a smaller binding energy.

3.1.3 Low energy electron diffraction

Low energy electron diffraction (LEED) is a very valuable tool to determine the surface structure of a sample^{40,42}. Electrons with a kinetic energy of 20 to 500 eV are used, which results in a de Broglie wavelength in the range of atomic distances ($\lambda = 0.05$ to 0.3 nm). Electrons with low kinetic energy interact strongly with the surface atoms. As a consequence they penetrate only 1-5 nm into the surface (cf. Figure 4b, page 10), which renders this technique highly surface sensitive. In the special case of ad-layers on surfaces the adsorbate unit cell can be determined with respect to the known substrate unit cell provided that the adsorbates show a long-range periodic ordering on the surface.

Figure 5a shows the set-up of a LEED system consisting of an electron gun, which emits electrons with variable energy, the grounded sample and the detection unit (four grids and a fluorescent screen). The first grid (counted from the sample) is grounded to insure a free field region around the sample. Grid two and three are held at slightly smaller biases than the kinetic energy of the electrons to repel the inelastically scattered electrons. Thus, only the elastically scattered electrons can pass the fourth grid and are then accelerated to the fluorescent screen, which is set to a high positive bias. Behind the screen a window in the UHV system equipped with a video camera allows direct recording of the diffraction pattern.

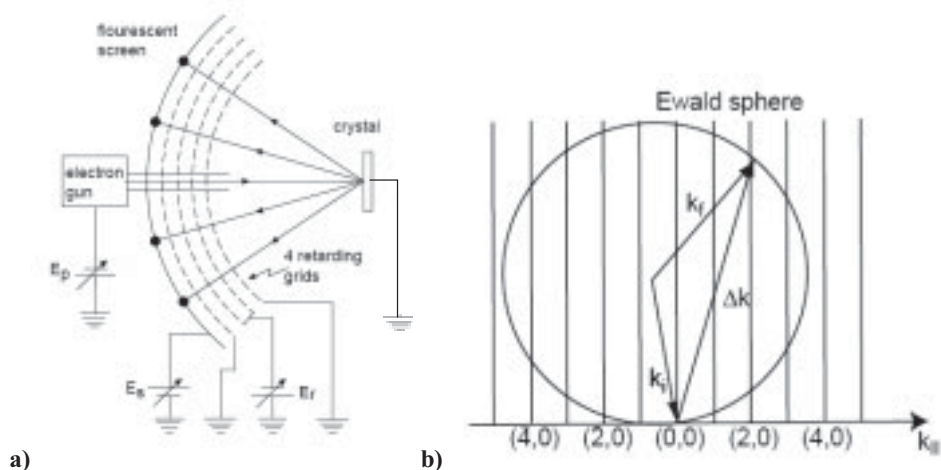


Figure 5: a) LEED system with the electron gun the crystal, the four retarding grids and the fluorescent screen; b) Ewald's sphere construction for diffraction from a 2D lattice; from⁴².